Separation and Purification Technology 173 (2017) 17–26

Contents lists available at ScienceDirect

Separation and Purification Technology

journal homepage: www.elsevier.com/locate/seppur

Clinoptilolite supported rutile TiO_2 composites: Synthesis, characterization, and photocatalytic activity on the degradation of terephthalic acid

H.B. Yener [a,*], M. Yılmaz [a], Ö. Deliismail [b], S.F. Özkan [b], Ş.Ş. Helvacı [a]

[a] Ege University, Faculty of Engineering, Department of Chemical Engineering, 35100 Bornova, Izmir, Turkey
[b] Izmir Institute of Technology, Faculty of Engineering, Department of Chemical Engineering, 35430 Urla, Izmir, Turkey

ARTICLE INFO

Article history:
Received 6 April 2016
Received in revised form 22 July 2016
Accepted 7 September 2016
Available online 9 September 2016

Keywords:
TiO_2
Clinoptilolite
Rutile
Titanium tetrachloride
Terephthalic acid
Photodegradation
Reusable catalyst

ABSTRACT

Clinoptilolite supported rutile TiO_2 composites were synthesized for the enhancement of its photocatalytic performance in the degradation of the aqueous terephthalic acid solution under UVC illumination by the increase in its surface area and to simplify its recovery from the treated solution after use. The XRD spectra of the composites revealed the formation of pure rutile TiO_2 on the surface of the clinoptilolite. The SEM images showed the formation of the spherical TiO_2 clusters were composed of nano fibers on the surface of the clinoptilolite. For all composites synthesized, the dispersion of the TiO_2 particles on the clinoptilolite led to a surface area larger than that of the bare TiO_2 and clinoptilolite. The materials synthesized in the present study exhibited higher catalytic activity compared with the commercial Degussa P25 and anatase. Among the catalysts synthesized the TiO_2/clinoptilolite with a weight ratio of 0.5 was found to be the most photoactive catalyst even though it contains a lesser amount of active TiO_2. The kinetic of the reactions for different catalyst was found to be consistent with the pseudo-first order kinetic model. The results of the Langmuir-Hinshelwood model showed the slight contribution of the adsorption on the degradation. The activity of the TiO_2/clinoptilolite with a weight ratio of 0.5 decreased after repetitive use due to the accumulation of the TPA molecules on the surface of the catalyst.

1. Introduction

The rapid growth in technology causes environmental problems both in the air and water. In order to overcome these issues, increased effort has been carried out to improve effective and inexpensive technologies. Heterogeneous photocatalytic degradation becomes a promising technology for the treatment of water because it is cheap and environmentally friendly. In this method, semiconductors are used as the photocatalyst and solar light as the energy, and the degradation reaction can be carried out under ambient conditions. The TiO_2 nano particles are one of the most preferred photocatalyst due to their low toxicity, chemical inertness, photostability, and high photocatalytic activity for the degradation of various organic compounds [1–3]. The crystal structure, size, shape, surface, and optical characteristic of the TiO_2 particles are crucial properties that affect their performances in photocatalytic degradation. Therefore, the studies regarding the synthesis of photoactive TiO_2 has gained interest in recent years. The main crystal structures of TiO_2, anatase, rutile, and brookite, show specific physical, chemical, and optical properties. Although TiO_2 nano particles exhibit high photocatalytic activity in the degradation reactions, recovery problems from the treated solution for reuse limits its application on an industrial scale. In order to improve their recovery from the treated solution they are dispersed on different kinds of supports having high adsorption capacity. The dispersion of TiO_2 on a support provides high specific surface area which enhances the degradation performance. The materials used as a support for TiO_2 particles are generally SiO_2 [4–9], activated carbon [10,11], and zeolites [2,3,12–15]. Among these supports, zeolites have attracted interest due to their unique structures, uniform pores, and channels [16–18]. Zeolites can be synthesized using different methods or obtained from natural sources. Although the properties of the synthetic zeolites can be easily tuned during the synthesis, natural zeolites are cheap, easily available, and abundant but require some chemical treatments to obtain a clean surface.

The TiO_2/zeolite composites are generally synthesized by the sol-gel, solvothermal and hydrothermal methods using organic and inorganic titanium precursors. Most of the composite synthe-

* Corresponding author.
E-mail address: huriye.banu.yener@ege.edu.tr (H.B. Yener).

http://dx.doi.org/10.1016/j.seppur.2016.09.010
1383-5866/

sis covers calcination at high temperatures (200–800 °C) to improve the crystal structure [2,3,13–17,19]. Since anatase is generally accepted as the most photoactive TiO_2, the studies generally focused on the calcination temperature for the formation of the anatase phase on a support [2]. However, due to the superior properties of rutile, that are thermodynamically stable and possess chemical inertness even in acidic and basic conditions, in recent years, the attraction to synthesize rutile TiO_2 has increased [1,20–24]. The synthesis of rutile TiO_2 generally consists of calcination at high temperatures for the transformation of the amorphous or anatase structures to rutile which increases the energy requirement and agglomeration of the particles. Therefore, the development of the methods and specifying the conditions for the synthesis of rutile TiO_2 with controlled properties at moderate conditions is important.

The studies regarding the synthesis of TiO_2 particles on clinoptilolite which is a natural zeolite generally consist of anatase TiO_2 particles obtained using $TiCl_4$ or TTIP as Ti precursor and calcination at high temperatures for phase change [3,14–17,19,25]. Trujillo et al. [14] studied the synthesis of anatase TiO_2/clinoptilolite composites using $TiCl_4$ as the titanium precursor with a final step of calcination at 400 °C and used them as a catalyst in the photocatalytic degradation of anionic and cationic contaminants. Wang et al. [15] synthesized clinoptilolite supported Cr-doped TiO_2 photocatalyst with a $TiCl_4$ precursor for the degradation of methyl orange under UVC illumination. They investigated the effects of the ion concentration and calcination temperature on the structure and photocatalytic activity of the composites. Petkowicz et al. [19] used zeolite NaA, synthesized using different silicon sources, as the support for the TiO_2 produced by $TiCl_4$ followed by calcination. Their photocatalytic activities were investigated in the degradation of methylene blue under UVA irradiation.

In the present study, the rutile TiO_2/clinoptilolite composites were synthesized by the hydrolysis of $TiCl_4$ on a clinoptilolite support at 95 °C and their photocatalytic activities were examined in the degradation of terephthalic acid (TPA) which is a raw material produced in millions of tones all over the world for the manufacture of polyester fibers and films [26]. The wastewater containing TPA may cause serious problems such as acute, chronic, and molecular toxicity to organisms [27,28]. The novelty of the present study is the synthesis of rutile TiO_2 particles on clinoptilolite at moderate temperature without calcination and their usage as catalyst in the degradation of TPA under UVC illumination which was not reported in literature before. The method and conditions in the present study provide a simple, one-step, and moderate temperature technique by which rutile TiO_2 particles can be synthesized with the desired properties without calcination.

2. Experimental

2.1. Materials

Titanium tetrachloride ($TiCl_4$, >99% purity, Merck) was used as a titanium precursor and hydrochloric acid (HCl, 38 wt%, Merck) as a solvent. Natural zeolite tuff (Gördes-Turkey) kindly supplied by INCAL MINERAL Co. was used as the support. Commercial Degussa P25 (30% rutile and 70% anatase), Rutile (Kronos) and Anatase (Sigma) were used as TiO_2 references. Terephthalic acid (TPA), with a high purity (>99.6%) was kindly supplied by PETKİM Petrochemical Co. and was selected as the model organic pollutant. All chemicals were used as received without further purification. The conductivity and pH of the double distilled water used in the study was 1.3 μS cm^{-1} and 6, respectively.

2.2. Preparation of the support

Natural zeolite tuff with a particle size of 5 cm was ground in a jaw crusher (Fritsch GmbH) and then wet sieved to ⩽38 μm. The tuff was purified using distilled water and HCl solution as given detailed in a previous study [29]. The elemental content of the natural zeolite was analyzed with an atomic absorption spectrophotometer (AAS, Varian SpectrAA-10Plus) and found that SiO_2, Al_2O_3, K_2O, and CaO in weight percentages of 75.5, 14.6, 5, and 3%, respectively, are the main components of the zeolite and the remaining contains trace amounts of other oxides such as Fe_2O_3, MgO, MnO, TiO_2, and Na_2O. Considering the Si/Al mole ratio (Si/Al = 4.38 > 4) [30] and the ratio of the sum of the divalent cations to the sum of the monovalent cations changing between 0.5 and 0.8 ($\sum M^{++}/\sum M^{+} = 0.58$) [31], the tuff is defined as clinoptilolite.

2.3. Synthesis of TiO_2 on clinoptilolite support

The TiO_2/clinoptilolite composites were synthesized by the acid hydrolysis of $TiCl_4$ on the clinoptilolite. The procedure reported by Yener and Helvacı [4,32] was followed for synthesis. Briefly, the aqueous solution of $TiCl_4$ (0.5 M) was prepared using HCl (3 M) to control the fast hydrolysis reaction of the $TiCl_4$ in water. In a typical synthesis, 250 mL of acidic $TiCl_4$ solution was added to the 20 and 10 g clinoptilolite for TiO_2/clinoptilolite weight ratios of 0.5 and 1, respectively, in a home-made reactor system. The hydrolysis reaction was carried out at 95 °C for 3 h, at a constant stirring rate of 500 rpm under reflux. After aging at room temperature for 24 h, the white precipitate and yellow supernatant were separated to analyze with AAS. The existence of Ti in the supernatant was evaluated as the unconsumed reactant of $TiCl_4$ and used for the calculation of the reaction efficiency. The other ions detected by AAS were the elements dissolved from the zeolite tuff due to the acidic reactant solution and resulted in a yellow supernatant. The precipitate was repeatedly washed with water to decrease the acidity of the suspension by removing the Cl ions until the pH of the rinsing water became neutral and then dried at 60 °C for 1 day. The composites synthesized at TiO_2/clinoptilolite weight ratios of 0.5 and 1 were denoted as TZ05 and TZ, respectively. Their photocatalytic activities were compared with those of the clinoptilolite and TiO_2 nano particles labeled as Z and T, respectively. The TiO_2 particles were synthesized using the same procedure without zeolite support under the same reaction conditions.

2.4. Characterizations

The quantitative analyses of the elements in the clinoptilolite and in the supernatant separated at the end of the composite synthesis were performed with X-ray fluourescence (XRF, Spectro IQ II) and an AAS analysis. The crystal structure of the particles was identified by X-ray diffraction (XRD, Philips X'pert PRO – 45 kV, 40 mA) with a 2θ ranging from 5 to 75° using Cu Kα radiation. The crystallite size of the particles was calculated using the Scherrer equation, $D = K\lambda/\beta\cos\theta$, where D is the crystallite size (nm), K is the crystallite-shape factor of 0.9, λ is the X-ray wavelength which is 0.15418 nm for CuKα, β is the X-ray diffraction broadening measured at half the line maximum intensity (radian), and θ is the diffraction angle (°) observed. The chemical structures of the products were specified by Fourier transform infrared spectroscopy (FTIR, Perkin Elmer Spectrum 100, Diamond/ZnSe crystals). The samples together with KBr (Sample: KBR = 1: 100 by weight) were pressed into pellets, and their analyses were performed at a resolution of 4 cm^{-1} over the 4000–600 cm^{-1} region in the transmittance mode. The specific surface areas and pore sizes of the samples were determined by means of N_2

adsorption-desorption isotherms at 77.35 K using a volumetric adsorption system (ASAP2010 Micromeritics Instrument). The samples were degassed at 300 °C based on the results of the thermo gravimetric analysis (Shimadzu TGA-51/51H) for 24 h prior to measurements to ensure that no gas molecules were adsorbed on the surface and in the pores of the particles. The shape and size of the particles were characterized by a field emission gun scanning electron microscope (SEM, FEI QUANTA 250 FEG). The diffuse reflectance spectra of the samples were obtained with a UV/Visible spectrophotometer equipped with an integrating sphere accessory (UV/Vis DRS, Schimadzu 2600) using $BaSO_4$ powder as a reference material. Their band gap energies (BGE) were estimated by transforming the diffuse reflectance spectrum into the equivalent absorption coefficient, which is proportional to the Kubelka-Munk function $F(R_\infty)$, $F(R_\infty) = (1 - R_\infty)^2/2R_\infty$, where R_∞ is the measured absolute reflectance from an infinitely thick layer of a sample $(R_\infty = R_{sample}/R_{standard})$ [33]. The indirect BGE was obtained from the plots of $(F(R_\infty)h\upsilon)^{1/2}$ versus $h\upsilon$ as the intercept of the extrapolated linear part of the plot at $(F(R_\infty)h\upsilon)^{1/2} = 0$. The zeta potentials of the materials were determined by means of the light scattering at different pH values (Malvern Zetasizer Nano ZS).

2.5. Photocatalytic experiments

The photocatalytic degradation of TPA was carried out in an aqueous medium in a homemade double walled borosilicate cylindrical batch reactor [34]. The temperature of the reaction medium was held constant at 25 °C by circulating cooling water in the jacket of the reactor. The irradiation was provided by a UVC lamp (Phillips G8T5, TUV 8 W, 254 nm) placed at the center of the reactor in a quartz tube. The reaction was performed with 20 ppm of 1 L of aqueous TPA solution with a pH 3.7 containing 0.75 g/L of catalyst. The uniformities in temperature, pH, and concentration of the solution during the reaction period were supplied by magnetic stirring. Prior to the photocatalytic degradation, the suspension was agitated for 1 h to reach adsorption-desorption equilibrium in the dark. The lamp was then switched on to initiate the photoreaction. The samples were taken at regular time intervals and placed into test tubes covered with aluminum foil and then centrifuged to remove the catalyst particles. In addition, a blank experiment without a catalyst was performed to elucidate the effect of photolysis. Both the photocatalytic experiments and their analysis were repeated at least three times in order to validate the results. The change in the concentrations of TPA and its probable degradation products with respect to irradiation time were determined using high performance liquid chromatography (HPLC, Shimadzu 20A) equipped with a UV–vis detector and an Inertsil ODS-4 column (5 μm, 250 mm × 4.6 mm). The mobile phase with a flow rate of 1 mL min^{-1} consisted of 90% 100 mM NaH_2PO_4 with a pH 2.1, 6% acetonitrile, and 4% water. The detection was monitored at 240 nm for TPA and at 210 nm for its degradation products. The quantitative analyses were performed on the base of the calibration curves using the software package of HPLC.

3. Results and discussion

3.1. Characterization of the particles and composites

The synthesis of the composites was conducted with a high aqueous acidic solution of HCl of 3 M which significantly affects the structure of the clinoptilolite [35]. Therefore, in order to determine the ions leached from the structure of the clinoptilolite, the supernatants were separated at the end of the synthesis of the composites of TZ and TZ05 to analyze with AAS (Fig. 1). For both composites, the most significant leaching was observed for magnesium. Even the silicon in the framework did not leach, 20% of aluminum was removed, and the Si/Al mole ratio of the clinoptilolite structure changed from 4.38 to 5.52 and 5.09 for TZ and TZ05, respectively. Thus, the structure of clinoptilolite was not destroyed during the synthesis of TiO_2/zeolite composites at the acidic conditions studied.

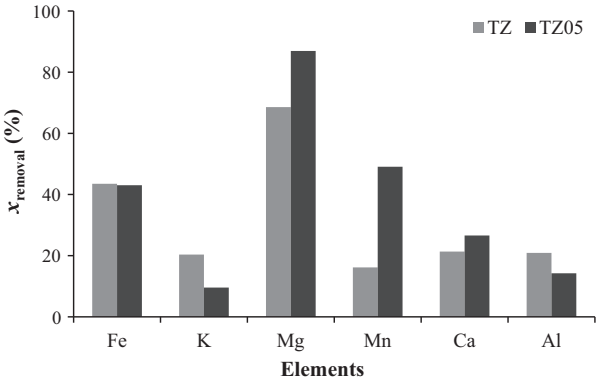

Fig. 1. Removal percentages of the elements, $x_{removal}$, separated from the clinoptilolite at the end of the composites synthesis.

The surface compositions of the composites in powder form determined by the XRF analysis shows that TiO_2 content of TZ surface was approximately double that of TZ05 as expected (Table 1). Elemental mapping was performed by SEM-EDS analysis to determine the distribution of the elements (Fig. 2) on the composites. The images showed that the coverage of TiO_2 particles in TZ is higher than that of TZ05 which is consistent with the XRF analysis.

The reaction efficiencies were calculated based on the Ti amount measured in the supernatant by assuming them as the unreacted Ti ions of the $TiCl_4$ solution. For the synthesis of both composites, the reaction efficiencies were found to be 97%, which confirms the assumption of 100% conversion of $TiCl_4$ to TiO_2 for the determination of the required amount of zeolite before the synthesis.

3.1.1. FTIR analysis

The FTIR spectra of the particles and clinoptilolite supported composites given in Fig. 3a show the bending vibrations of the sorbed water at around 1640 cm^{-1}. In the FTIR spectrum of Z, the band at 1070 cm^{-1} is assigned to the O—Si(Al)—O asymmetric stretching vibrations of the zeolite structures [14,36,37] and the symmetric vibration of Si—O—Si at 800 cm^{-1} [12]. The FTIR spectrum of T shows the stretching vibration of Ti—O and Ti—O—Ti bands below 1000 cm^{-1}. In the FTIR spectra of the composites, the characteristic zeolite band at 1070 cm^{-1} slightly shifts towards a higher wave number by keeping the zeolite structure unchanged. This slight shift was explained by the addition of the transition metal cations into a zeolite structure during the synthesis [36,37]. In addition, its intensity decreased due to the increase in the TiO_2 content. Similar to the FTIR spectrum of T, the broad band below 1000 cm^{-1} attributed to the Ti—O—Ti bonds confirm the formation of the TiO_2 structures on the zeolite for TZ05 and TZ. The intensity of the band at 800 cm^{-1} decreased for TZ05 and disappeared for TZ with the increase in the TiO_2 content. This may be explained by the overlapping of the Si—O—Si band of zeolite and Ti—O band of TiO_2.

3.1.2. XRD analysis

The XRD patterns of the particles and composites are given in Fig. 3b. The XRD spectrum of the zeolite indicated the characteristic peaks (2θ = 9.83, 22.33, 25.95, 26.69, 29.86, and 31.75°) of the

Table 1
Surface chemical composition (wt%) of the composites.

Composites	MgO	Al_2O_3	SiO_2	K_2O	TiO_2	MnO	Fe_2O_3
TZ05	0.32	4.48	51.98	0.84	40.90	0.02	0.29
TZ	0.41	2.12	16.44	0.08	80.08	0.04	0.05

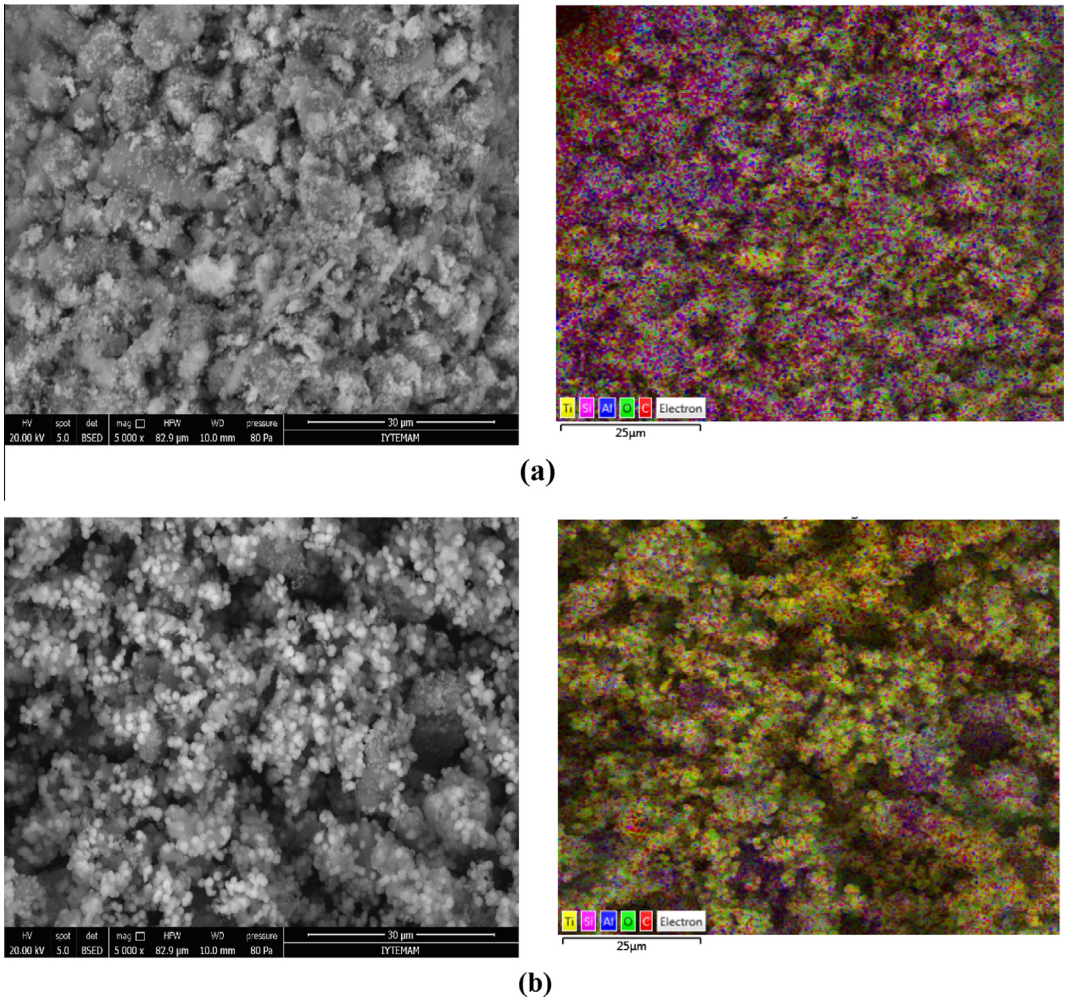

Fig. 2. Elemental mapping of the (a) TZ05, (b) TZ by SEM-EDS analysis.

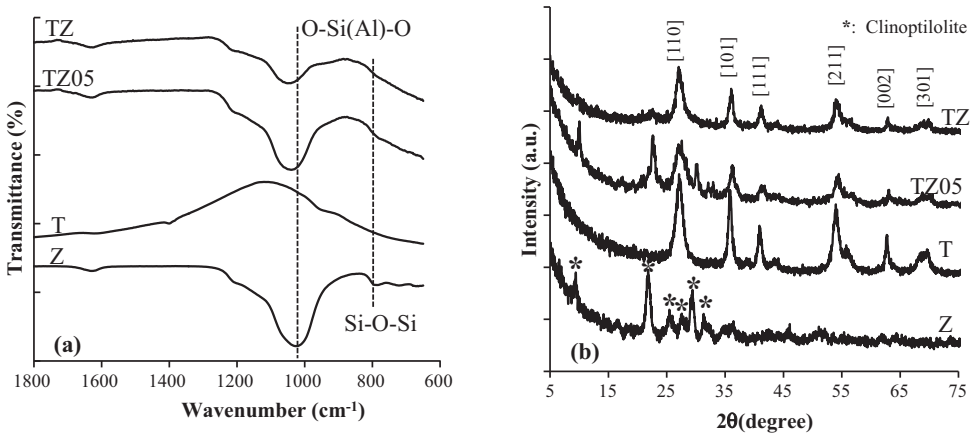

Fig. 3. (a) FTIR and (b) XRD patterns of the particles and composites.

clinoptilolite minerals which are found to be consistent with the chemical analysis, and quartz ($2\theta = 26°$) as the impurity [17,37]. The XRD pattern of the TiO_2 denoted that all of the diffraction peaks can be assigned to a well crystallized rutile TiO_2 which corresponds to the data listed in JCPDS No 77-0441. The peaks of other crystallite phases of TiO_2, anatase and brookite, were not observed indicating synthesis of a pure rutile phase at the conditions studied. In the XRD spectrum of TZ05, the characteristic peaks of both the clinoptilolite and rutile phases were observed. However, their intensities are lower than that of the clinoptilolite and TiO_2. The peaks corresponding to the clinoptilolite observed in the XRD patterns of TZ05 supported the stability of the clinoptilolite structure even after the high acidic reaction. This result is consistent with that obtained from the chemical analysis. On the other hand, the XRD spectrum of TZ shows dominantly the characteristic peaks of the rutile phase and slightly the peak of clinoptilolite at $2\theta = 22.33°$. It may be suggested that since the amount of TiO_2 synthesized was higher in TZ than that of TZ05, they almost covered the surface of the clinoptilolite and hindered the peaks of the clinoptilolite from being detected by XRD. An increase in the TiO_2 content in the TZ increased the intensity of the rutile peaks compared with that of TZ05. The crystallite size was calculated using the Scherrer equation (Table 2). The crystallite size increased with an increase in the TiO_2 content at the conditions studied.

3.1.3. N_2 adsorption-desorption analysis

The textural properties of the Z, T, TZ05, and TZ obtained from the N_2 adsorption-desorption isotherms are given in Table 2. The crystallite size of the TiO_2 particles are bigger than the pore size of the clinoptilolite (d_{pore}), so they are formed on the surface of the clinoptiolite crystals rather than inside the pores, and the composites (TZ05 and TZ) have higher total surface areas than clinoptilolite (Z). The TZ has a higher external surface area than the TZ05 indicating that the mesoporous structure is dominant and the pores are larger than the TZ05. On the other hand, the TZ05 still has a microporous structure due to the uncovered clinoptilolite crystals by TiO_2.

3.1.4. SEM analysis

The SEM images of the clinoptilolite (Fig. 4a) showed the relatively smooth surface of the clinoptilolite crystals in grave shape. As given in Fig. 4b, the agglomerates of the TiO_2 particles consist of spherical particles. Previous studies showed that, these spheres were formed by the interconnected nano fibers growing from a center in a radial direction [4]. Since the size of these nano fibers are quite homogeneous, the surface of the spheres formed by the tips of the nano fibers seems very smooth. The surface of the natural zeolite was covered by the spherical TiO_2 clusters and became rough for both composites (Fig. 4c and d). An increase in the weight ratio of the TiO_2/clinoptilolite from 0.5 to 1 increased both the coverage of TiO_2 clusters on the surface of the zeolite and the TiO_2 agglomeration. The change in the coverage with respect to the weight ratio was supported with the surface chemical compositions of the composites obtained by XRF (Table 1) and SEM-EDS (Fig. 2.) analyses. As seen from the images, the TiO_2 particles were synthesized on the surface of the clinoptilolite rather than its pores. The size of the TiO_2 clusters on the surface of the zeolite for both weight ratios were found to be smaller than that of pure TiO_2. Similar to the TiO_2/SiO_2 composites synthesized by Yener and Helvaci [4], the presence of the clinoptilolite in the reaction medium or formation of the Ti—O—Si band during the composite synthesis delayed the formation of the TiO_2 nuclei and may hinder the growth of the particles.

3.1.5. UV–vis DRS analysis

The UV–vis DRS spectra of the TiO_2 particles and TiO_2/clinoptilolite composites are given in Fig. 5. Their band gaps obtained from the plots of the Kubelka-Munk function given as an inset in Fig. 5 are summarized in Table 2. The decrease in the TiO_2 content resulted in a slight shift in the diffuse reflectance of the composites towards shorter wavelengths and consequently with a slight increase in the band gap energy in comparison with that of the bare TiO_2.

3.1.6. Zeta potential measurements

The zeta potentials of the materials synthesized as a function of the solution pH are given in Fig. 6. The zeta potential of the bare clinoptilolite at the pH range studied was found to be highly negative which was also reported by Trujillo et al. [14] and Liu et al. [17]. The trend in the zeta potential of Z with respect to the pH was found to be similar to that of TZ05 due to the low amount of TiO_2 particles on the surface of the clinoptilolite. The surface charges of the composites were found to be positive at a low pH due to the presence of TiO_2 on the surface of the clinoptilolite and decreased with the increase in pH. The isoelectric points of T, TZ05, and TZ were found to be 4.75, 2.15, and 5.50, respectively. The isoelectric point of TiO_2 particles are generally found to be between 6 and 7 in literature. The difference in the isoelectric point given in literature and found in this study may be due to the variation in the synthesis methods and reaction conditions during the synthesis.

3.2. Photocatalytic reactions

3.2.1. Effect of the amount and type of the photocatalyst

The catalytic activities of the particles and composites synthesized in the present study were determined in the photocatalytic degradation of TPA. The photocatalytic degradation was performed at 25 °C, in 1 L of an aqueous TPA solution of which the concentration and pH are 20 ppm and 3.7, respectively. As it is well known, the characteristic properties of the catalysts like the surface area, surface charge, crystal structure and size, and the reaction conditions such as the type and concentration of the pollutant, the pH of the solution, the catalyst amount, and the type of the photon source highly affect the efficiency of the photocatalytic reactions. In the present study, in order to elucidate the effects of the

Table 2
The structural properties of the particles and TiO_2/clinoptilolite composites.

Sample	Crystallite size[a] (nm)	Total surface area[b] (m^2/g)	External surface area[b] (m^2/g)	d_{pore} (nm)	BGE (eV)
T	6.8	93	89	2.9[c]	3.04
Z	10.1	23	6	0.9[d]	–
TZ05	5.3	194	74	1.1[d]	3.10
TZ	6.4	210	120	2.6[c]	3.08

[a] Crystallite size was calculated by the Scherrer Equation using XRD data at $2\theta = 27°$ for [1 1 0] plane of rutile and $2\theta = 22.3°$ for zeolite.
[b] Total and External surface areas were calculated by BET and t-plots methods.
[c] Mesopore average diameter was derived using BJH method.
[d] Micropore median diameter was derived using Horvath-Kawazoe method.

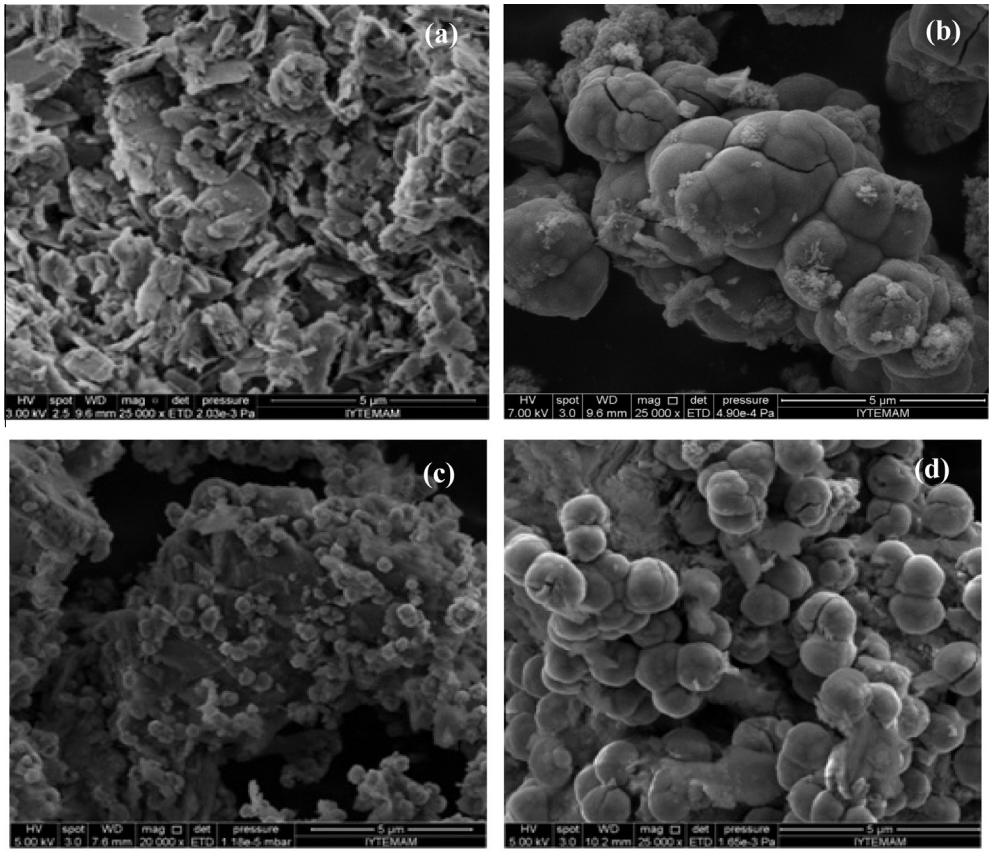

Fig. 4. SEM images of the (a) Z, (b) T, (c) TZ05, and (d) TZ.

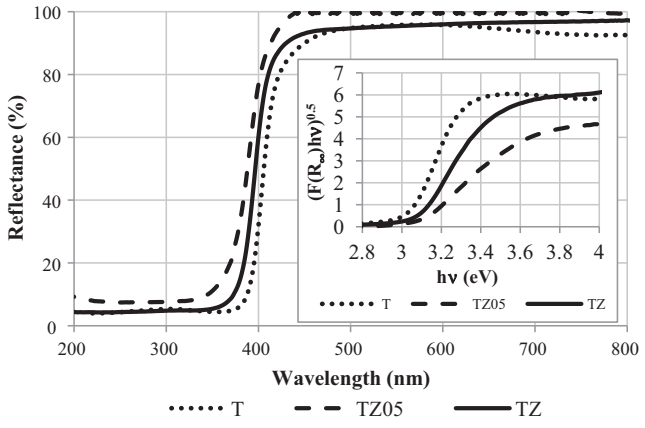

Fig. 5. Diffuse reflectance spectra and plots of the modified Kubelka-Munk function (*inset*).

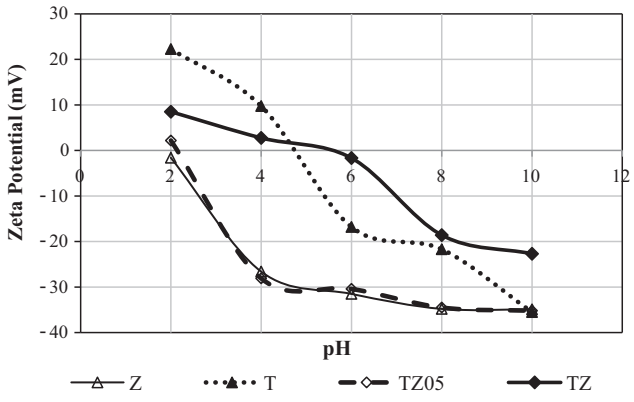

Fig. 6. The Zeta potentials of the particles and composites with respect to pH.

characteristic properties of the catalysts on the degradation, the reaction conditions were kept constant. Prior to the photocatalytic degradation, that is before the UVC lamp was switched on, the adsorption-desorption equilibrium was satisfied for 1 h. The amounts of adsorbed TPA on the materials were found to be changing between 5% and 15%. This pointed out the slight contribution of adsorption to the removal of TPA and the need of the photolysis reaction for the further degradation of TPA.

The photocatalytic experiments were performed to determine the optimum amount of catalysts for T, TZ05 and TZ with four loadings of 0.1, 0.5, 0.75 and 1 g/L of which results are given in Fig. 7. The overall degradation percentages, $X\%$ were calculated as $X\% = (C_0 - C)/C_0 \times 100$ where C_0 is the concentration at the end of the adsorption-desorption equilibrium stage and C is the remaining TPA concentration in the treated solution at the end of the reaction time of 2 h. For the catalyst of T, the degradation increased up to 0.75 g/L and then decreased at a catalyst amount of 1 g/L. For the supported catalysts of TZ05 and TZ, no significant change in the degradation was observed up to the 0.75 g/L and a similar decrease in degradation was observed at 1 g/L. The decrease in the degradation at 1 g/L catalyst amount might be due to the light scattering effect which hinders the penetration of UV light through the solution and reduction in the surface area of TiO_2 being exposed to light illumination [3,4,27]. Since high degradation was obtained and no significant change in the degradation was observed at the catalyst amount of 0.75 g/L for all catalysts investigated, the optimum catalyst amount was selected as

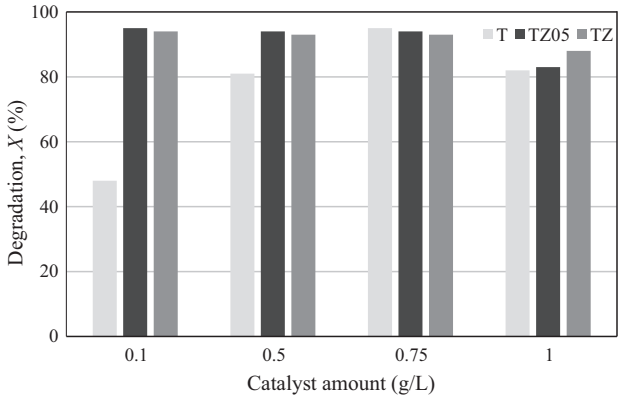

Fig. 7. Effect of catalyst dosage on the degradation of TPA (C_0 = 20 ppm).

0.75 g/L, and all other investigations were performed with this catalyst amount.

The normalized concentration of TPA versus time is given in Fig. 8a where C_0 is the TPA concentration measured at the end of the adsorption-desorption equilibrium and C_t is the remaining TPA concentration in the treated solution at irradiation time t. In order to determine the role of the photolysis on the degradation, an experiment was carried out without any catalyst (photolysis). The photolysis achieved only a 10% degradation of TPA. In the reactions where clinoptilolite was used as catalyst, a similar degradation with photolysis, 11%, was observed, indicating that clinoptilolite alone is not effective in the photocatalytic degradation of TPA. The pH of the solution is one of the main factors that

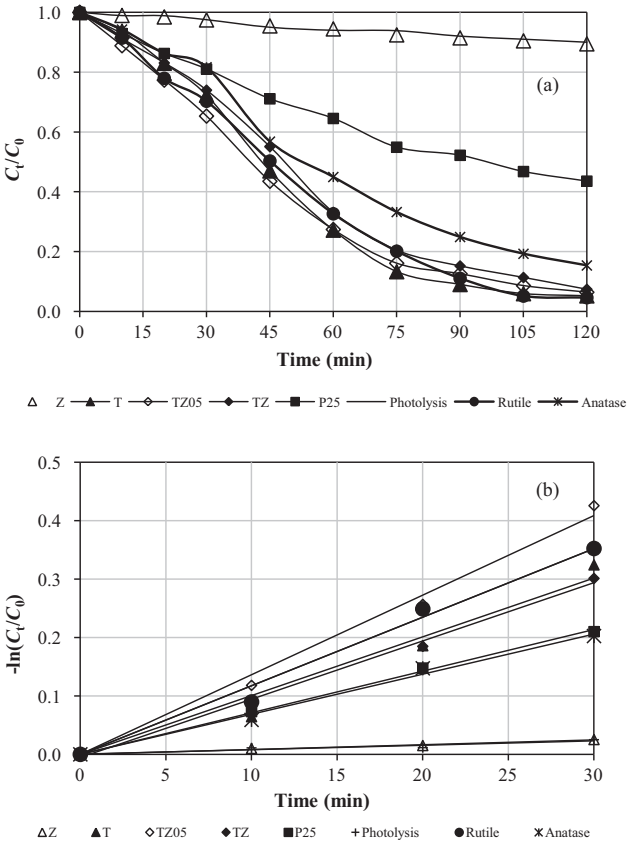

Fig. 8. (a) The normalized concentration versus irradiation time, and (b) $-\ln(C_t/C_0)$ vs. irradiation time (Catalyst amount: 0.75 g/L, C_0 = 20 ppm).

influence the ionization degree of the organic pollutant and the surface charge of the catalysts. TPA has two carboxylic groups with pKa values of 3.52 and 4.82 [27]. At a pH > 3.52 one of the carboxylic groups started to dissociate its proton and became negatively charged. Thus, with the pH of the solution as 3.7, the TPA was partially ionized. The surface charge of the bare clinoptilolite at the pH studied was found to be negative (Fig. 6) which led to a reduction in the electrostatic attraction between the ionized TPA and surface of the clinoptilolite. Both the negative charge and low surface area of the clinoptilolite (Table 2) resulted in a low adsorption of the pollutant TPA on its surface where the photocatalytic reaction takes place and consequently low photocatalytic degradation.

The photocatalytic activities of the composites with two different TiO_2/clinoptilolite weight ratios of 0.5 and 1 were investigated. The degradation percentages were found to be 94 and 93% for TZ05 and TZ, respectively. The degradation rate increased compared with the photolysis alone and the reaction where clinoptilolite was used as catalyst. Although the catalytic activity of clinoptilolite alone was very low, it does not affect the photocatalytic activity of the TiO_2 on the composites. No significant difference in the degradation percentage with respect to the TiO_2 content was observed and both composites obtained almost the same degradation value at the end of the irradiation time. The similarity in the degradation for both composites can be explained by comparing their characteristic properties. Since the photocatalytic reactions commonly occur on the surface of the catalyst, surface area is one of the most crucial properties affecting the photocatalytic degradation. As seen in Table 2, the surface areas of both composites were found to be similar to each other. Another property affecting the catalytic activity is the surface charge. The surface charges of TZ05 and TZ were found to be negative and positive, respectively, at the pH studied. The negative surface charge of TZ05 reduced the attraction between its surface and ionized TPA whereas, the positive charge of TZ favored this attraction. Another effect that plays an important role in degradation is the size and distribution of the TiO_2 particles on the clinoptilolite surface. TiO_2 particles with a smaller size and with a homogeneous distribution covered the clinoptilolite surface, and less agglomeration was observed in the TZ05 than that of TZ (Fig. 4c and d). Eventually, the assessment of the characteristic properties indicated that for the nearly close surface areas, the homogeneous TiO_2 distribution on the clinoptilolite of the TZ05 compensated for the negative effect of the surface charge in the degradation, and similar photocatalytic degradation percentages, 94% for TZ05 and 93% for TZ, were obtained for both composites with the conditions studied. The photocatalytic activities of the composites were compared with that of the pure TiO_2 synthesized. As shown in Fig. 8a, T showed nearly the same degradation as that of the composites. While the same catalyst concentrations of 0.75 g/L were used in the experiments, the TiO_2 contents of the composites were naturally lower than that of the pure TiO_2 which were 1/2 for TZ and 1/4 for TZ05. The low content of TiO_2 in the composites decreased the active sites activated by the UV irradiation compared with the pure TiO_2. However, the high surface area of the composites may enhance the adsorption of the TPA molecules on the surface of the composites leading to the same degradation with a decreased amount of photoactive TiO_2. Even so, the same photocatalytic degradation of TPA was obtained for the composites at the end of 2 h of reaction. In addition, the removal of the composites from the treated solution after irradiation is easier than the pure TiO_2 which provides the reuse of the catalysts [3,4]. In order to compare the photocatalytic activities of the materials synthesized, commercial TiO_2 in different crystal structures (the mixture of rutile and anatase, rutile and anatase) were examined in the photocatalytic degradation of TPA. Although there are a lot of studies reported the excellent photocatalytic activity of Degussa P25

and the anatase TiO_2 particles used in different degradation reactions [3,38–41], in the degradation of TPA with the reaction conditions used in this study, the commercial (Rutile) and synthesized (T) rutile exhibited better catalytic performances than commercial anatase rutile mixture (P25) and commercial anatase (Anatase) (Table 3). The same catalyst may exhibit different photocatalytic activity depending on the type of the pollutant [14,42,43]. The high photocatalytic degradation percentages obtained in the presence of the materials synthesized and commercial rutile confirmed the superior photocatalytic ability of the rutile phase for the degradation of TPA. Similar results for the photocatalytic degradation of TPA under UVC irradiation were reported by Yener and Helvaci [4] for the rutile TiO_2 particles dispersed on the amorphous SiO_2 obtained from rice husk ash.

The photocatalytic reaction of most organic compounds at low initial concentrations is described by the pseudo-first order kinetic model by assuming the homogeneous reaction as [27]

$$-r_0 = -\frac{dC_0}{dt} = kC_0 \quad (1)$$

where r_0 is the initial rate of TPA in the photocatalytic reaction and k is the pseudo-first order reaction rate constant. Since no degradation byproducts were detected by the HPLC analysis of which chromatogram is given as a Supplementary Material, the experimental data obtained for the first 30 min of the degradation reaction were fitted to the linearized form of the Eq. (1) and is seen in Fig. 8b. The slopes of the straight lines give the reaction rate constants of each reaction for different catalysts and are given in Table 3. The high regression coefficient (Table 3) revealed the suitability of the pseudo-first order kinetic model assumption. Although nearly the same degradation was obtained at the end of the 2 h illumination time for T, TZ05 and TZ, the reaction rate constants indicated that the rate of degradation is in the order of TZ05 > TZ > T.

The photocatalytic activities of the catalysts were also investigated using the turnover frequency (TOF) which was calculated using the slope of the kinetic curves of all the catalysts studied at zero time per mole of Ti in the catalysts (Table 3) [4]. The trend in TOF was found to be similar with the trend in the first order reaction rate constant, k and overall degradation efficiency, X. The TOF of the composites were higher than the TiO_2 particles which indicated the increase in the rate of degradation. Similarly, the TOF increased with the decrease in TiO_2 amount in the composites.

TOF per effective TiO_2 surface area of the supported catalysts was also calculated. As explained in Section 3.1.3, since the TiO_2 particles were synthesized on the surface of the clinoptilolite crystals rather than inside the pores, the external surface area of the composites was taken as the effective surface area of the TiO_2 particles. The TOF per TiO_2 surface area were calculated as 0.00015, 0.00025 and 0.00011 min^{-1} m^{-2} TiO_2 for T, TZ05 and TZ, respectively. The results were found to be consistent with that of TOF calculated per mol of Ti, indicating the increase in the rate of degradation with the use of composites and with the decrease in the TiO_2 amount in the composites.

3.2.2. Effect of the initial concentration of TPA

Among the catalysts studied, TZ05 was found to be the most photoactive catalyst considering its low TiO_2 content, high degradation percentage and high TOF value. Thus, the effect of the initial concentration of TPA on the degradation efficiency was studied at four different initial concentrations of TPA using TZ05 as a catalyst by keeping the other reaction conditions constant. The change in the concentrations with respect to the irradiation time is seen in Fig. 9a. The amount of pollutant adsorbed on the surface of the catalyst is expected to increase with an increase in the concentration of pollutant solution leading to the high degradation percentage [16,25]. On the other hand, a high concentration may hinder the penetration of UV light to the catalyst surface and reduce the degradation rate [16]. The degradation percentages of the 2 h of reaction were found to be 94, 88, 64, and 52% for TPA concentrations of 20, 40, 80, and 100 ppm, respectively. As a result, for higher degradation percentages more irradiation time is needed for TPA concentrations of 80 and 100 ppm. In order to determine the role of the adsorption on the photocatalytic degradation, the Langmuir-Hinshelwood model describing the heterogeneous reaction occurring at a solid-liquid interface was used [12,25,44]

$$-r_0 = -\frac{dC_0}{dt} = \frac{k_r K_{add} C_0}{1 + K_{add} C_0} \quad (2)$$

where K_{add} and k_r are the equilibrium adsorption constant and degradation constant at maximum coverage, respectively. The r_0 values were independently obtained from the concentration versus irradiation time curves seen in Fig. 9a by the linear fit using only the experimental points during the first 30 min of irradiation. The linearized form of the Langmuir-Hinshelwood model equation was used to plot the data given in Fig. 9b. The values of K_{add} and k_r were obtained from the intercept and slope of the linear fit as 0.016 ppm^{-1} and 1.02 min^{-1} ppm, respectively. The reaction rate constant was calculated by multiplication of K_{add} and k_r and found as 0.0166 min^{-1}. For TZ05, the reaction rate constant obtained for the pseudo-first order reaction model, 0.0136 min^{-1} and the Langmuir-Hinshelwood model, 0.0166 min^{-1} were found to be close to each other indicating the slight contribution of adsorption on photolysis.

3.2.3. Reusability of the catalyst

A catalyst recycling study was conducted using TZ05 as catalyst with a TPA concentration of 20 ppm and catalyst amount of 0.75 g/L to determine the reusability of the catalyst over three cycles. At the end of the first cycle, the catalyst was centrifuged, washed several times with distilled water, dried at 60 °C and reused in the second cycle. The same treatment procedure was applied after the second use. A decrease in the photocatalytic degradation efficiency was observed with respect to the repeated usage as seen in Fig. 9c.

Table 3
Results of photodegradation of TPA.

Sample code	k (min^{-1})	R^2	Degradation, X (%)	TOF (min^{-1} mol^{-1} Ti)
T	0.0101	0.967	95	1.08
Z	0.0008	0.984	11	–
TZ05	0.0136	0.991	94	5.80
TZ	0.0097	0.996	93	2.07
P25*	0.0071	0.998	56	0.76
Rutile*	0.0117	0.987	95	1.25
Anatase*	0.0069	0.992	85	0.74
Photolysis	0.0008	0.905	10	–

* Degussa P25 TiO_2; Kronos TiO_2; Sigma TiO_2.

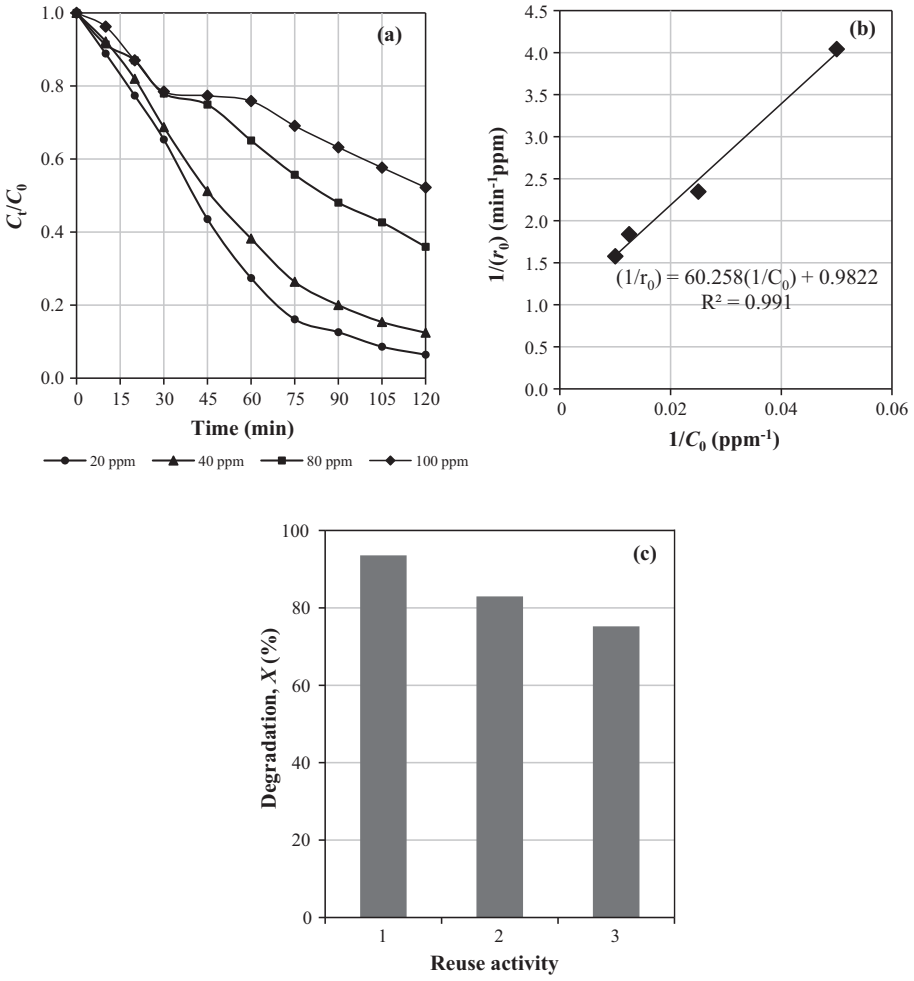

Fig. 9. (a) Change in the concentration with respect to the irradiation time at different initial TPA concentrations, (b) Linearization of the Langmuir Hinshelwood model equation, and (c) Degradation percentage as a function of the number of use (Catalyst: TZ05, Catalyst amount: 0.75 g/L).

The degradation efficiencies were found to be 94, 88, and 75% for the first, second, and third cycles, respectively. The reduction in the photocatalytic activity was probably due to the accumulation of TPA on the surface of the catalyst. This may reduce the adsorption due to the blockage of the active sites by the pollutant molecules and consequently lower the photocatalytic activity. Kanakaraju et al. [3] also reported a reduction in the photocatalytic activity for the degradation of amoxicillin due to the blockage of the pollutant and its degradation byproducts on the surface and pores of the TiO_2/clinoptilolite catalyst. Gomez et al. [2] also observed a reduction in the activity of the TiO_2/HZSM-11catayst after repetitive usage. In order to generate the activity of the catalyst, they calcined the recovered catalyst. However, since the synthesis procedure in the present study does not include calcination which significantly affects the properties of the particles, the catalyst was not calcined for regeneration.

4. Conclusion

Rutile TiO_2/clinoptilolite composites were synthesized by the acid hydrolysis of a $TiCl_4$ solution at TiO_2/clinoptilolite weight ratios of 0.5 and 1 at 95 °C without calcination. At the weight ratio of 1, the agglomeration of the TiO_2 particles was found to be higher than that of 0.5 by conserving the shapes of the clusters as spheres consisting of the interconnected nano fibers. The synthesis of TiO_2 particles on the clinoptilolite led to the formation of the composites with a high surface area. All the catalysts synthesized in the study exhibited high photocatalytic activity. The composites satisfied the high precipitation rate which simplifies the recovery of the catalyst from the treated solution for reuse. Among the catalysts used the TiO_2/clinoptilolite composites with a weight ratio of 0.5 was found to be the most appropriate catalyst for the degradation of TPA since it provided the same degradation rate with its low TiO_2 content. The experimental data of the reactions with different types of the catalysts was fitted to the pseudo-first order kinetic model which described the degradation behavior of TPA with high correlation coefficients. In addition, the Langmuir-Hinshelwood model showed the slight contribution of the adsorption to the degradation. The photocatalytic activity of the TiO_2/clinoptilolite composites with a weight ratio of 0.5 decreased 20% after three repetitive use due to the blockage of TPA on the surface of the composites.

Acknowledgements

This project was supported by The Scientific and Technological Research Council of Turkey (TUBITAK) through Projects 104M255 and 110M451, and The Science, Technology Application, and Research Center of Ege University (EBILTEM) through Project 2012/BIL/027, The Scientific Research Council of Ege University through project 13MUH031. The authors also thank PETKIM Petrochemical Co. for the TPA and INCAL Mineral Co. for natural zeolite tuff.

Appendix A. Supplementary material

Supplementary data associated with this article can be found, in the online version, at http://dx.doi.org/10.1016/j.seppur.2016.09.010.

References

[1] Y. Cao, X. Li, Z. Bian, A. Fuhr, D. Zhang, J. Zhu, Highly photocatalytic activity of brookite/rutile TiO2 nanocrystals with semi-embedded structure, Appl. Catal. B 180 (2016) 551–558.

[2] S. Gomez, C.L. Marchena, L. Pizzio, L. Pierella, Preparation and characterization of TiO2/HZSM-11 zeolite for photodegradation of dichlorvos in aqueous solution, J. Hazard. Mater. 258–259 (2013) 19–26.

[3] D. Kanakaraju, J. Kockler, C.A. Motti, B.D. Glass, M. Oelgemöller, Titanium dioxide/zeolite integrated photocatalytic adsorbents for the degradation of amoxicillin, Appl. Catal. B 166–167 (2015) 45–55.

[4] H. Banu Yener, Ş.Ş. Helvacı, Effect of synthesis temperature on the structural properties and photocatalytic activity of TiO2/SiO2 composites synthesized using rice husk ash as a SiO2 source, Sep. Purif. Technol. 140 (2015) 84–93.

[5] M. Bonne, S. Pronier, F. Can, X. Courtois, S. Valange, J.-M. Tatibouët, S. Royer, P. Marécot, D. Duprez, Synthesis and characterization of high surface area TiO2/SiO2 mesostructured nanocomposite, Solid State Sci. 12 (2010) 1002–1012.

[6] T. Cetinkaya, L. Neuwirthová, K.M. Kutláková, V. Tomášek, H. Akbulut, Synthesis of nanostructured TiO2/SiO2 as an effective photocatalyst for degradation of acid orange, Appl. Surf. Sci. 279 (2013) 384–390.

[7] L. Pinho, F. Elhaddad, D.S. Facio, M.J. Mosquera, A novel TiO2–SiO2 nanocomposite converts a very friable stone into a self-cleaning building material, Appl. Surf. Sci. 275 (2013) 389–396.

[8] D. Sannino, V. Vaiano, P. Ciambelli, G. Carotenuto, M. Di Serio, E. Santacesaria, Enhanced performances of grafted VOx on titania/silica for the selective photocatalytic oxidation of ethanol to acetaldehyde, Catal. Today 209 (2013) 159–163.

[9] Y. Yang, F. Su, S. Zhang, W. Guo, X. Yuan, Y. Guo, Fabrication of metallic platinum doped ordered mesoporous titania–silica materials with excellent simulated sunlight and visible light photocatalytic activity, Colloids Surf., A 415 (2012) 399–405.

[10] S. Basha, C. Barr, D. Keane, K. Nolan, A. Morrissey, M. Oelgemoller, J.M. Tobin, On the adsorption/photodegradation of amoxicillin in aqueous solutions by an integrated photocatalytic adsorbent (IPCA): experimental studies and kinetics analysis, Photochem. Photobiol. Sci.: Official J. Euro. Photochem. Assoc. Euro. Soc. Photobiol. 10 (2011) 1014–1022.

[11] T.T.H. Yoneyama, Titanium dioxide/adsorbent hybrid photocatalysts for photodestruction of organic substances of dilute concentrations, Catal. Today 58 (2000) 133–140.

[12] S. Gomez, C.L. Marchena, M.S. Renzini, L. Pizzio, L. Pierella, In situ generated TiO2 over zeolitic supports as reusable photocatalysts for the degradation of dichlorvos, Appl. Catal. B 162 (2015) 167–173.

[13] C. Lazau, C. Ratiu, C. Orha, R. Pode, F. Manea, Photocatalytic activity of undoped and Ag-doped TiO2-supported zeolite for humic acid degradation and mineralization, Mater. Res. Bull. 46 (2011) 1916–1921.

[14] M.E. Trujillo, D. Hirales, M.E. Rincón, J.F. Hinojosa, G.L. Leyva, F.F. Castillón, TiO2/clinoptilolite composites for photocatalytic degradation of anionic and cationic contaminants, J. Mater. Sci. 48 (2013) 6778–6785.

[15] C. Wang, H. Shi, Y. Li, Synthesis and characterization of natural zeolite supported Cr-doped TiO2 photocatalysts, Appl. Surf. Sci. 258 (2012) 4328–4333.

[16] S. Khodadoust, A. Sheini, N. Armand, Photocatalytic degradation of monoethanolamine in wastewater using nanosized TiO2 loaded on clinoptilolite, Spectrochim. Acta Part A Mol. Biomol. Spectrosc. 92 (2012) 91–95.

[17] S. Liu, M. Lim, R. Amal, TiO2-coated natural zeolite: rapid humic acid adsorption and effective photocatalytic regeneration, Chem. Eng. Sci. 105 (2014) 46–52.

[18] M.A. O'Neill, F.L. Cozens, N.P. Schepp, Photogeneration and migration of electrons and holes in zeolite NaY, J. Phys. Chem. B 105 (2001) 12746–12758.

[19] D.I. Petkowicz, R. Brambilla, C. Radtke, C.D.S. da Silva, Z.N. da Rocha, S.B.C. Pergher, J.H.Z. dos Santos, Photodegradation of methylene blue by in situ generated titania supported on a NaA zeolite, Appl. Catal. A 357 (2009) 125–134.

[20] B. Cao, W. Yao, C. Wang, X. Ma, X. Feng, X. Lu, Simple fabrication of rutile titanium dioxide whiskers, Mater. Lett. 64 (2010) 1819–1821.

[21] D. Dolat, D. Moszyński, N. Guskos, B. Ohtani, A.W. Morawski, Preparation of photoactive nitrogen-doped rutile, Appl. Surf. Sci. 266 (2013) 410–419.

[22] A. Heciak, A.W. Morawski, B. Grzmil, S. Mozia, Cu-modified TiO2 photocatalysts for decomposition of acetic acid with simultaneous formation of C1–C3 hydrocarbons and hydrogen, Appl. Catal. B 140–141 (2013) 108–114.

[23] S. Kamimura, T. Miyazaki, M. Zhang, Y. Li, T. Tsubota, T. Ohno, (Au@Ag)@Au double shell nanoparticles loaded on rutile TiO2 for photocatalytic decomposition of 2-propanol under visible light irradiation, Appl. Catal. B 180 (2016) 255–262.

[24] J. Orlikowski, B. Tryba, J. Ziebro, A.W. Morawski, J. Przepiórski, A new method for preparation of rutile phase titania photoactive under visible light, Catal. Commun. 24 (2012) 5–10.

[25] E.C. Ilinoiu, R. Pode, F. Manea, L.A. Colar, A. Jakab, C. Orha, C. Ratiu, C. Lazau, P. Sfarloaga, Photocatalytic activity of a nitrogen-doped TiO2 modified zeolite in the degradation of Reactive Yellow 125 azo dye, J. Taiwan Inst. Chem. Eng. 44 (2013) 270–278.

[26] Z.J. Wang, L.H. Teng, J. Zhang, X.L. Huang, J.F. Zhang, Study on optimal biodegradation of terephthalic acid by an isolated Pseudomonas sp., Afr. J. Biotechnol. 10 (2011) 3143–3148.

[27] A. Shafaei, M. Nikazar, M. Arami, Photocatalytic degradation of terephthalic acid using titania and zinc oxide photocatalysts: comparative study, Desalination 252 (2010) 8–16.

[28] X.X. Zhang, S.L. Sun, Y. Zhang, B. Wu, Z.Y. Zhang, B. Liu, L.Y. Yang, S.P. Cheng, Toxicity of purified terephthalic acid manufacturing wastewater on reproductive system of male mice, Mus musculus, J. Hazard. Mater. 176 (2010) 300–305.

[29] Ö. Deliismail, Preparation of Natural Zeolite Supported TiO2 Composites for Removal of Terephthalic Acid, Izmir Institute of Technology Engineering, 2014.

[30] A.R. Ruiz-Salvador, D.W. Lewis, J. Rubayo-Soneira, G. Rodrı·guez-Fuentes, L.R. Sierra, C.R.A. Catlow, Aluminum distribution in low Si/Al Zeolites: dehydrated Na-clinoptilolite, J. Phys. Chem. B 102 (1998) 8417–8425.

[31] A. Alietti, Polymorphism and crystal-chemistry of heulandites and clinoptilolites, Am. Miner. 57 (1972) 1148–1462.

[32] H.B. Yener, Ş.Ş. Helvacı, Visible light photocatalytic activity of rutile TiO2 fiber clusters in the degradation of terephthalic acid, Appl. Phys. A 120 (2015) 967–976.

[33] I. Tunc, M. Bruns, H. Gliemann, M. Grunze, P. Koelsch, Bandgap determination and charge separation in Ag@TiO2 core shell nanoparticle films, Surf. Interf. Anal. 42 (2010) 835–841.

[34] H.B. Yener, Synthesis of Titanium Dioxide Nano Particles and Their Photocatalytic Activities on Degradation of Terephthalic Acid (TPA), Graduate School of Applied and Natural Sciences, Ege University, 2011.

[35] F. Cakicioglu-Ozkan, S. Ulku, The effect of HCl treatment on water vapor adsorption characteristics of clinoptilolite rich natural zeolite, Microporous Mesoporous Mater. 77 (2005) 47–53.

[36] D.W. Breck, Zeolite Molecular Sieves: Structure, Chemistry and Uses, John Wiley & Sons, New York, 1974.

[37] A. Nezamzadeh-Ejhieh, F. Khodabakhshi-Chermahini, Incorporated ZnO onto nano clinoptilolite particles as the active centers in the photodegradation of phenylhydrazine, J. Ind. Eng. Chem. 20 (2014) 695–704.

[38] Y. Gao, H. Wang, J. Wu, R. Zhao, Y. Lu, B. Xin, Controlled facile synthesis and photocatalytic activity of ultrafine high crystallinity TiO2 nanocrystals with tunable anatase/rutile ratios, Appl. Surf. Sci. 294 (2014) 36–41.

[39] F. Xu, W. Xiao, B. Cheng, J. Yu, Direct Z-scheme anatase/rutile bi-phase nanocomposite TiO2 nanofiber photocatalyst with enhanced photocatalytic H2-production activity, Int. J. Hydrogen Energy 39 (2014) 15394–15402.

[40] G. Zhang, Y.C. Zhang, M. Nadagouda, C. Han, K. O'Shea, S.M. El-Sheikh, A.A. Ismail, D.D. Dionysiou, Visible light-sensitized S, N and C co-doped polymorphic TiO2 for photocatalytic destruction of microcystin-LR, Appl. Catal. B 144 (2014) 614–621.

[41] L. Zhu, K. Liu, H. Li, Y. Sun, M. Qiu, Solvothermal synthesis of mesoporous TiO2 microspheres and their excellent photocatalytic performance under simulated sunlight irradiation, Solid State Sci. 20 (2013) 8–14.

[42] M.R. Eskandarian, M. Fazli, M.H. Rasoulifard, H. Choi, Decomposition of organic chemicals by zeolite-TiO2 nanocomposite supported onto low density polyethylene film under UV-LED powered by solar radiation, Appl. Catal. B 183 (2016) 407–416.

[43] V. Likodimos, A. Chrysi, M. Calamiotou, C. Fernández-Rodríguez, J.M. Doña-Rodríguez, D.D. Dionysiou, P. Falaras, Microstructure and charge trapping assessment in highly reactive mixed phase TiO2 photocatalysts, Appl. Catal. B 192 (2016) 242–252.

[44] F.F. de Brites-Nobrega, A.N. Polo, A.M. Benedetti, M.M. Leao, V. Slusarski-Santana, N.R. Fernandes-Machado, Evaluation of photocatalytic activities of supported catalysts on NaX zeolite or activated charcoal, J. Hazard. Mater. 263 (Pt 1) (2013) 61–66.